Laser-Powered Vibrotactile Rendering

YUNING SU, Simon Fraser University, Canada
YUHUA JIN, Simon Fraser University, Canada
ZHENGQING WANG, Simon Fraser University, Canada
YONGHAO SHI, Simon Fraser University, Canada
DA-YUAN HUANG, Simon Fraser University, Canada
TENG HAN, Institute of Software, Chinese Academy of Sciences, China
XING-DONG YANG, Simon Fraser University, Canada

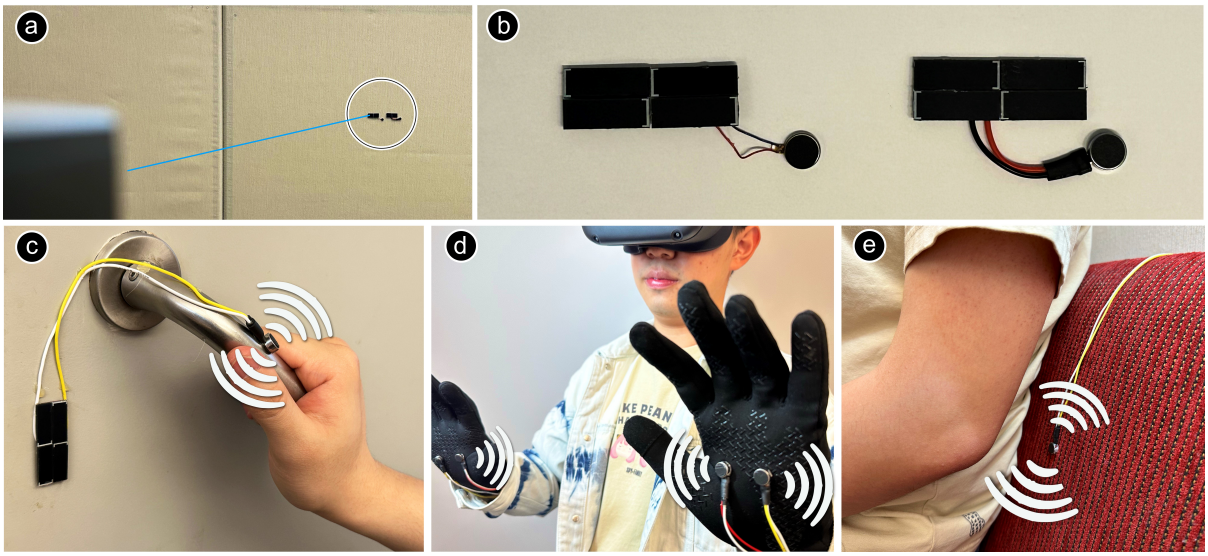

Fig. 1. Top row: illustration of our battery-free, electronic-free vibrotactile device. (a) The device is powered and controlled by a laser, avoiding the need for frequent charging or battery replacement. (b) The device is made up of solar cells connected to a linear resonant actuator (LRA) or eccentric rotating mass (ERM) motor. Bottom row: application scenarios for prolonged device operation. (c) A door handle with ambient haptic feedback to show if the room is occupied. (d) Haptic gloves for immersive VR experiences. (e) An ambient haptic display on a coach to remind a user of important upcoming meetings.

Authors' addresses: Yuning Su, Simon Fraser University, British Columbia, Canada, yuning_su@sfu.ca; Yuhua Jin, Simon Fraser University, British Columbia, Canada, mit.yuhua@gmail.com; Zhengqing Wang, Simon Fraser University, British Columbia, Canada, zwa170@sfu.ca; Yonghao Shi, Simon Fraser University, British Columbia, Canada, yonghao_shi@sfu.ca; Da-Yuan Huang, Simon Fraser University, British Columbia, Canada, da-yuan_huang@sfu.ca; Teng Han, Institute of Software, Chinese Academy of Sciences, Beijing, China, hanteng@iscas.ac.cn; Xing-Dong Yang, Simon Fraser University, British Columbia, Canada, xingdong_yang@sfu.ca.

2474-9567/2023/12-ART178
https://doi.org/10.1145/3631449

We investigate the feasibility of a vibrotactile device that is both battery-free and electronic-free. Our approach leverages lasers as a wireless power transfer and haptic control mechanism, which can drive small actuators commonly used in AR/VR and mobile applications with DC or AC signals. To validate the feasibility of our method, we developed a proof-of-concept prototype that includes low-cost eccentric rotating mass (ERM) motors and linear resonant actuators (LRAs) connected to photovoltaic (PV) cells. This prototype enabled us to capture laser energy from any distance across a room and analyze the impact of critical parameters on the effectiveness of our approach. Through a user study, testing 16 different vibration patterns rendered using either a single motor or two motors, we demonstrate the effectiveness of our approach in generating vibration patterns of comparable quality to a baseline, which rendered the patterns using a signal generator.

CCS Concepts: • **Human-centered computing → Haptic devices**.

Additional Key Words and Phrases: Haptics, Energy Harvesting, Virtual Reality

ACM Reference Format:
Yuning Su, Yuhua Jin, Zhengqing Wang, Yonghao Shi, Da-Yuan Huang, Teng Han, and Xing-Dong Yang. 2023. Laser-Powered Vibrotactile Rendering. *Proc. ACM Interact. Mob. Wearable Ubiquitous Technol.* 7, 4, Article 178 (December 2023), 25 pages. https://doi.org/10.1145/3631449

1 INTRODUCTION

Small and lightweight electromagnetic actuators, such as LRAs and ERM motors, have widespread usage in AR/VR and ubiquitous computing applications for providing rich vibrotactile feedback. However, the requirement for regular battery charges or replacements presents a considerable challenge for their deployment in daily use cases that require extended system operation. In recent years, battery-free technologies have emerged as a promising solution, with actuators that operate using alternative sources such as light [22] or kinetic energy [46] exhibiting the potential to enable prolonged device operation. However, the incorporation of energy harvesting and power management components, in addition to the already cumbersome electronics and hardware, results in a trade-off that yields a bulky device form factor that may be intrusive when deployed on everyday objects or uncomfortable to wear on the human body.

In this paper, we examine the viability of developing a vibrotactile device comprising small ERM motors or LRAs without requiring any batteries or electronic components, such as microcontrollers, driver chips, or Wi-Fi modules. Our approach involves using a laser as a wireless power transfer and haptic control mechanism, enabling the actuators to be driven using DC (e.g., ERM) or AC (e.g., LRA) signals. The proposed method replaces the battery with small PV cells that harness laser energy at any distance across a room. Additionally, electronic components required for power management and motor control, including drivers, microcontrollers, and other hardware, are removed. Instead, the intensity or duty cycle of the laser is used to control the rendering of different vibrational patterns. The outcome is a simple and low-maintenance device architecture, as illustrated in (Figure 1a-b).

In contrast to alternative wireless charging approaches such as magnetic induction, lasers are capable of operating over long distances with minimal attenuation. Compared to far-field technologies including microwaves [55] and radio-frequency identification (RFID) [38], as well as optical methods utilizing visible light [49], lasers have high power density, leading to a smaller form factor for the haptic device that is crucial in daily applications. Additionally, lasers offer directional transmission, which enables the precise control and focused delivery of power to a particular device.

We studied the influence of several critical parameters on the effectiveness of our method using a blue laser operating within the range of 200mW to 600mW and a wavelength of 445 nm. We found that parameters such as beam size and angle of incidence exhibited negligible influence on generated vibrotactile output. Additionally, by examining the correlation between laser input intensity and PV cell output voltage, we determined that a laser power of 500mW with a beam size of $368mm^2$ is the optimal choice in our implementation for achieving a balance

between low laser power and richness of haptic output. Using this optimal power choice, we develop a proof-of-concept prototype that operates within the safety range of the laser-induced damage threshold (LIDT) [16], with a power density of $135.9 mW/cm^2$, similar to that of direct sunlight. Despite the relatively low conversion efficiency of the PV cells (i.e., only 10%), our prototype is capable of energizing an ERM motor or LRA to generate some of the most common vibrotactile patterns. By rapidly sweeping between the adjacent PV cells of two motors, our prototype can even activate two motors simultaneously (with a reduced maximum intensity), thereby creating richer effects, such as the illusion of vibration passing across the space between the motors [14], using a single laser source.

We present several use cases (see Figure 1c-e) and the result of a user study involving seven participants, in which we evaluated the rendering quality of our method against a baseline method using a signal generator. We tested 9 vibration patterns rendered using a single ERM motor and 7 patterns rendered using two ERM motors. The results of our study indicate that our approach was able to generate vibration patterns of comparable quality to the baseline, thus providing evidence of the potential for laser-powered vibrotactile rendering.

The contributions of our work include (1) introduction of using laser as a mechanism to power and control vibrotactile actuators; (2) validation of technical feasibility through a working prototype; (3) insights into critical parameters that affect our proposed method; and (4) demonstration of the effectiveness of our approach through a user study.

2 RELATED WORKS

Our study is situated within the literature concerning the application of vibrotactile feedback, primarily in smart virtual and physical environments, as well as energy harvesting and wireless power transfer techniques, and battery-free interactive systems.

2.1 Vibrotactile Output

Vibrotactile output has gained widespread adoption in commercial products, leveraging phones, handheld controllers, or vests to offer an immersive experience, especially in AR/VR applications [3, 12, 48]. Given their compact form factor, lightweight, and affordability, vibration motors have also become a popular tool for researchers seeking to explore novel means of interaction with the virtual world across various regions of the human body.

For example, providing vibrotactile feedback on the palm or fingers can foster improved interaction with virtual environments by detecting the virtual object's touch [19], tracking its movement [30], or perceiving its deformation through sensations of stretching, bending, and twisting [15]. The torso is also a widely studied area for receiving the vibrotactile output [9]. For example, vibrating on the chest and back of the body could create an illusion of something passing through the body [15]. In addition to the hand and torso, vibrotactile output rendered on the head has been shown to provide effective relief for motion sickness [39] or communicate information for 3D navigation [27].

2.2 Harvesting and Transferring Power Wirelessly

2.2.1 Energy harvesting. An instinctive strategy for energizing a compact haptic device is leveraging sunlight. However, the operation of an ERM motor necessitates intense and constant sunlight, which is not ensured even during daylight hours. As an alternative, the conversion of body heat via Peltier elements is plausible, but the power output generated is limited to the micro-watt range [29], inadequate to supply the energy requirements of an ERM motor. In contrast, kinetic energy generated from body movement provides a more substantial energy output but this approach may result in quicker user fatigue [41].

2.2.2 Wireless power transfer. Transferring power wirelessly can be accomplished through various means, such as magnetic resonance coupling, electromagnetic induction, microwave, and laser, each presenting distinct features that vary in terms of efficiency, power, and range. Magnetic resonance coupling, for instance, is suitable for working in close proximity, thus, suitable for smartphones and other small devices [2]. The efficiency of electromagnetic induction is also subject to a decline as distance increases [32]. In contrast, microwaves can cover greater distances but are hard to be used in indoor environments due to their dependence on large antennas and high-power levels to attain adequate efficiency [45]. The omnidirectional nature of microwaves also poses a challenge in our application context, where precise control of individual vibration motors is essential.

In comparison to these technologies, lasers have unique benefits owing to their capability to provide concentrated energy with precise targeting over long distances. In outdoor settings, lasers have demonstrated their utility in charging unmanned aerial vehicles (UAVs) [6], robots [21, 28], and satellites [31]. Within indoor environments, lasers have been employed to wirelessly charge an individual [20] or several smartphones simultaneously [51]. To ensure usability across a wide range of IoT devices, laptops, and smartphones, practical guidelines have been established for the implementation of distributed laser charging systems [52]. Additionally, safety systems have been developed to promptly deactivate the laser in response to user exposure, with a reaction time of under 300 μs [20].

2.3 Battery-Free Interative Devices

Battery-free input devices have been developed by using kinetic energy generated by user interaction with a device, such as pushing a button [34] or twisting a knob [1]. Recent advancements have expanded on this approach by demonstrating that a Gameboy console can be powered solely through the energy harvested from button clicks and ambient light [8]. In the realm of augmented reality, Li and Zhou have developed a gaze-tracking system powered by thin film solar cells [33].

Regarding output devices, prior studies have investigated the viability of utilizing the energy produced from a user's rubbing motion on an electret harvester to power LEDs or e-ink displays [26]. Another common technology that can generate a small amount of electricity is triboelectric nanogenerators (TENGs) [50], which have been used to stimulate nerve fibers within the skin to create electro-tactile output [44]. For the purpose of generating higher levels of energy, Teng and Lopes [47] developed a haptic device that can provide long-term use of vibration and electrical stimulation by harnessing the energy from arm movement. Pulsed lasers have also been used to induce a sensation of strain through thermoelastic deformation of the skin [25], but their effectiveness has yet to be established. It is worth noting that incorporating power management components, drivers, and microcontrollers for vibration motors may increase device form factor and complexity. Our goal is to examine the feasibility of vibrotactile devices that do not rely on batteries or electronics.

3 WORKING PRINCIPLE

In the simplest form, our system comprises a small actuator connected to one or two solar cells, which harvests laser energy from a laser source installed on the ceiling or wall of a room. Since there is no need for a battery, circuits and components relating to power management are no longer needed. Our approach can drive both AC and DC vibration motors, including LRA and ERM motors, commonly used in AR/VR and ubiquitous computing applications.

3.1 Controlling ERM Motors Using DC Signals

Controlling a single ERM motor. A single ERM motor can be controlled through a single laser source (Figure 2b). Since the solar cell generates DC power, the intensity of the motor's vibrations can be adjusted by regulating the power of the laser, with greater laser power resulting in higher speeds and hence, more intense vibrations.

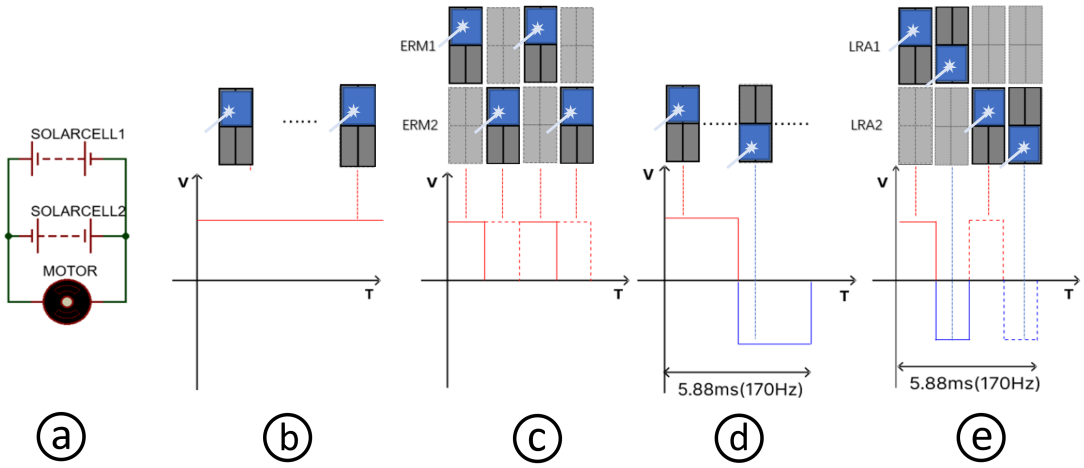

Fig. 2. Working principle of our vibration device, which is powered by a laser. (a) The connection scheme of our prototype, wherein two solar cells are connected in opposite directions. Cell 1 generates a positive signal, represented by the red color, while Cell 2 produces a negative signal, indicated by the blue color. For DC signals, Cell 2 is used to counteract the impact of ambient light. (b) Pointing the laser at Cell 1 generates DC signals for a single ERM motor. (c) Controlling two ERM motors by evenly distributing the laser duty cycle between the solar cells of different motors. (d) Sequentially scanning Cell 1 and Cell 2 generates AC signals for a single LRA. (e) Controlling two LRA motors by distributing the duty cycle between Cell 1 and Cell 2, as well as between the solar cells of different motors.

Since there is no need for signal or data handling on the haptic device, the controller unit (e.g., microcontroller or driver chip), data communication unit (e.g., Wi-Fi module), and all the other electronic components are removed.

Controlling multiple ERM motors. A single laser source can sequentially scan the solar cells of different actuators to drive the motors in an alternating manner (referred to as alternating patterns in this paper). However, in scenarios that demand simultaneous control of multiple motors, employing multiple laser sources may be necessary (referred to as concurrent patterns). Alternatively, simultaneous control of more than one ERM motor can be achieved by the rapid sweeping of the laser beam between adjacent solar cells of different motors (Figure 2d). This method requires rapid transfer of the laser beam to the adjacent motor after achieving the desired vibration intensity in the current motor and promptly returning before any significant decay in the current motor (Figure 8). We demonstrate the feasibility of this approach by using it to control the simultaneous actuation of two ERM motors, resulting in richer vibration patterns such as simulating a moving object between the two motors (i.e., vibrotactile flow [42]). Note that conventional methods employing electric components necessitate a designated driver chip for each individual motor for control.

The limitation of this approach is that the time of exposure to the laser for each solar cell decreases by a factor equivalent to the number of motors, leading to a proportional decrease in the maximum vibration intensity of each motor. However, it should be noted that the reduction in intensity does not necessarily equate to a proportionate reduction in haptic experience, as the accuracy of the vibration intensity must be appropriately aligned with the corresponding virtual event.

3.2 Controlling LRAs Using AC Signals

Controlling a single LRA. Unlike the simpler ERM motor, controlling an LRA is challenging due to the need for AC signals. The current method for LRA control involves converting DC signals produced by solar cells into AC

signals using a PV inverter. Our method eliminates the need for the PV inverter by incorporating an additional solar cell connected in parallel but in the opposite direction (Figure 2a). This arrangement generates an AC signal when a laser beam sequentially scans the two solar cells (Figure 2c). We used square waves for simplicity in our implementation. The frequency of the produced AC signal can be optimized by adjusting the speed at which the laser beam sweeps to align with the resonant frequency of the LRA (170 Hz in our implementation). The power of the laser can be modulated to adjust the amplitude of the vibrations. One of the advantages of using LRAs instead of ERM motors is their shorter rise time. Our experimental results demonstrate that the transition time of the rising and falling edge of the signal generated using our method is around 10 microseconds, which is significantly shorter than the period of typical AC signals (1ms) used for common vibrotactile output. This fast transition time is comparable to what can be achieved using electronics, ensuring a smooth and effective control of the vibrations of the LRA.

Controlling multiple LRAs. Similar to the simultaneous control of ERMs, simultaneous control of multiple LRAs, each with distinct vibrational intensities, can be achieved through the use of a single laser source that quickly scans the solar cells of different LRA at their respective resonant frequencies (Figure 2e). In this case, the vibration intensity of an LRA is also influenced by the duration of exposure of its solar cells to the laser beam (duty cycle), in addition to the laser power. If the laser power is held constant, an increased duty cycle engenders a stronger vibration.

3.3 Operate Against the Impact of Ambient Light

An important consideration in our design is to minimize the impact of ambient light as the addition of ambient light to the laser power may result in unpredictable fluctuations in output voltage, making it difficult to precisely control motor vibration. Particularly, in situations where high levels of ambient light intensity prevail, such as direct exposure to sunlight, the power density may exceed $130 mW/cm^2$, surpassing the threshold required to directly power an ERM motor, thereby rendering the control of motor vibration infeasible. To address this issue, an additional PV cell (i.e. SOLARCELL2 in Figure 2) can be introduced to the current setup with a polarity opposite to that of the existing cell. This configuration would offset the energies of both cells, effectively neutralizing each other's output when exposed to equal levels of ambient light. It is worth noting that the same cell arrangement is used for powering the LRAs. Hence, the impact of ambient light on the LRAs is minimal. The difference is that, unlike the LRAs, the additional PV cell used for the ERM motors does not serve the purpose of receiving energy from the laser.

3.4 Braking

To enhance the clarity of vibrotactile rendering, haptic drivers commonly incorporate a reverse signal to brake the motor. One widely utilized haptic driver for this purpose is the DRV2605 [18]. In our implementation of the system, an alternative braking mechanism can be achieved using lasers, thereby eliminating the need for a haptic driver or any additional components. This novel approach entails directing the laser at the opposing cell to achieve the desired braking effect. For example, if the laser is focused on the PV cell utilized to counteract the impact of ambient light, it will generate a negative DC signal, effectively acting as a brake for the DC motor. Similarly, by scanning the laser at the cells of the LRAs in a reversed sequence, the system can generate an opposing AC signal, which effectively brakes the LRAs..

4 IMPLEMENTATION

We present the implementation details of our prototype, which comprises two main components: a laser source and a haptic device composed of a vibration motor(s).

4.1 Haptic Device

Our haptic device was implemented using two different types of motors: a 3V 11000RPM ERM motor and a 2.5V 170Hz LRA, both of which are commonly used in research and commercial products. The ERM motor is controlled using DC, while the LRA is controlled using AC signals. The motor is connected to low-cost PV cells from Anysolar (KXOB25-14X1F), each with dimensions of 23×8 mm. These cells exhibit good performance when exposed to high power-density light sources, making them well-suited for use with lasers. The cells are composed of monocrystalline material and are capable of harnessing visible light as well as a segment of the near-infrared spectrum with consistent conversion efficiency.

The PV cells are connected in parallel but oriented in the opposite direction. It should be noted that this setup alone produces a maximum 690mV for the ERM motor and an average root mean square voltage (Vrms) of 585 mV for the LRA, which is inadequate to generate strong vibrations. To address this issue, we incorporated an additional PV cell in each direction, connected in series, to increase the maximum output power to 1310mV DC for the ERM motor and 1100 mV (AC, Vrms, square wave) for the LRA. While adding more cells could further increase the output power, it would result in an undesirable increase in the device's size. Therefore, we opted to use only two cells in each direction (four in total), as the current output capacity is adequate for driving the LRA or ERM motor to generate vibrations of varying strengths, suitable for a range of applications, such as simulating engine vibrations or a butterfly alighting on the palm.

Considering cell placement, a stable surface, such as a wall or the side panel of a couch, can provide a solid foundation for the installation of PV cells, particularly when used to augment everyday objects. However, this setup may not be the optimal choice for wearable scenarios due to the need for tethering the haptic device to moving body parts. An alternative approach involves affixing the PV cells to a wearable item, like a glove or vest. In this case, precise tracking of the cells' motion is necessary to ensure accurate alignment with the cell. Recent technological advancements in computer vision have made it possible to track tagged objects with millimeter-level accuracy and millisecond-scale latency [37]. Given this, we've made the strategic choice not to delve into the implementation of a motion-tracking system within the confines of our current work. A more detailed discussion of potential tracking systems that could integrate with our method is outlined in Section 9.

4.2 Laser

We utilized a rectangular blue laser diode with a wavelength of 445 nm and a maximum output power of 700mW. In the final implementation, however, the output power was set to 500mW according to the results of our experiments. The movement of the laser beam was controlled using a galvo scanner. We used the blue laser primarily for debugging and illustration purposes, while a near-infrared laser is preferred due to its lower risk of ocular damage.

Laser safety. Ensuring compliance with the Maximum Permissible Exposure (MPE) limit is crucial in protecting users from potential laser-induced hazards [16]. In our implementation, we took a strategy to mitigate the power density by increasing the beam size to match the dimensions of the two PV cells, which is $368mm^2$. The resulting power density is $135.9mW/mm^2$, which is similar to the power density of direct sunlight ($\sim 135mW/cm^2$) and is 32.1% lower than the laser-induced damage threshold of $200mW/cm^2$, the MPE value calculated for our continuous 445nm laser. We based our calculations on the American National Standard for Safe Use of Lasers (ANSI Z136) [16], taking into account the potential for prolonged skin exposure of up to 10^4 seconds. Note that the beam size can be increased using a beam expander or by increasing the distance between the laser diode and the cells. While the former approach is preferred, as it allows the power density to remain at the same low level along the pathway of the beam, the latter approach was chosen as a cheaper alternative in our initial explorations.

Overdrive. In low voltage conditions, the ERM motor exhibits a delay of approximately 300ms before it reaches the desired vibration intensity. A common approach to reducing this rise time is to introduce a brief period of

overdrive at a higher voltage. Overdrive is also used to produce low-intensity vibration when the input power is below 400mW, which is inadequate to nitiate motor spinning. The overdrive is commonly supplied through a driver chip with conventional electronic components. In our prototype, we incorporated a 10ms 500mW laser (outputting 1310mV) as a prefix to the lasers with power levels below 400mW to realize overdrive. On the other hand, overdrive is not required for the LRA. Our implementation employs an LRA with a very short rise time of roughly 11.8ms, even when driven by a minimum power of a 50mW laser. This time is less than two duty cycles of the LRA's resonant frequency (170Hz).

5 EXPERIMENTS

We conducted a series of experiments to assess the potential impact of several critical parameters such as beam size, angle of incidence, and laser power on the performance and viability of our approach. Furthermore, we were interested in understanding whether the commonly used methods to enhance the performance of inexpensive vibration motors, such as overdriving, can be effectively achieved using the laser. Our investigation intentionally excluded application-specific questions, such as the feasibility of tracking the movement of solar cells, as they fall outside the scope of this initial exploration. Particularly, we sought to answer the following questions:

Q1: How does beam size impact output voltage? If a negligible impact is found, larger beam sizes are preferred for reduced power density or improved safety.

Q2: How does the angle of incidence of a beam may affect the output voltage? If the impact is significant, meticulous setup and calibration may be necessary, which can be costly and time-consuming.

Q3: How does laser power level impact output voltage? The answer will allow us to understand how to render vibration intensities of varying degrees.

Q4: Can the rise time of the ERM motor be significantly reduced with our overdrive implementation? Our focus of this question has been deliberately limited to the ERM motors, as the rise time is of less concern in the case of LRAs.

5.1 How Does Beam Size Impact Output Voltage?

The first question we sought to answer was the impact of beam size on the energy harvested by the PV cells. The experiment setup involved the placement of PV cells at a perpendicular angle to a laser beam of 200mW. To achieve different beam sizes, the distance between the laser source and the PV cells was manually adjusted. The beam size was increased from $8mm^2$ to $88mm^2$ with increments of $10mm^2$, with the maximum size selected to fit within the shape of a single PV cell. We ensured that there was no overflow beyond the edge of the PV cell which allowed complete absorption of the laser power by the PV cell. To account for potential variations in the conversion efficiency across the PV cell's surface, the beam's position was randomly altered within the cell.

Results. Our result suggests that the size of the laser beam exhibited negligible influence on the amount of energy harvested by the PV cells. This is evidenced by the relatively constant voltage output ranging from 600mV to 612mV for the ERM motor and from 470mV to 471mV Vrms for the LRA, observed across varying beam sizes (Figure 3). We anticipate that this outcome can be generalized to larger beams and cells, given the identical internal structure of the PV cells. As noted previously, it is crucial to maintain the size of the beam above a safe threshold, which is determined based on power density (and kept below LIDT) to ensure safety. Hence, a larger beam dimension is preferred. However, beams that are excessively larger than the cell should be avoided to allow for the capture of all available energy. Based on the finding of this study, we selected a beam size of approximately $368cm^2$, which covers the combined area of two PV cells.

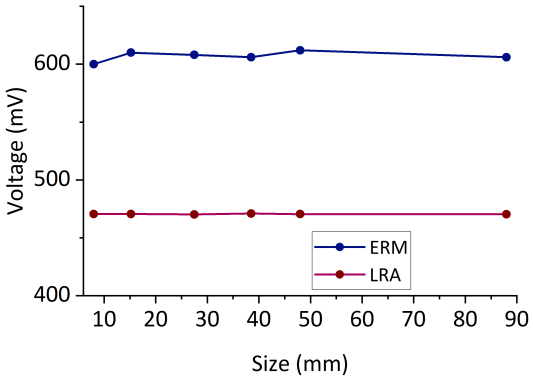

Fig. 3. Voltage output of the ERM motor and LRA (Vrms) with different sizes of the laser beam.

5.2 How Does Angle of Incidence Impact Output Voltage?

This study aimed to measure the impact of the angle of incidence on the output voltage of the PV cells. The study setup was similar to the first study, except that the PV cells were placed at a fixed location 2m away from the laser source. We varied the angle of incidence from -80° to 80° with a step of 10°. To ensure the beam remained within the boundaries of the PV cells' surface area across the different angles of incidence, the size of the laser beam was adjusted to an area of $27.5cm^2$.

Results. Our results indicate that the angle of incidence of the laser had negligible effects on the harvested energy. We observed a stable voltage output range of 588mV to 614mV for the ERM motor and 470mV to 470.6mV Vrms for the LRA across all tested angles of incidence (Figure 4). Our findings are consistent with previous investigations of sunlight, which have demonstrated that a perpendicular alignment between the laser and solar cell is not a necessary condition for efficient energy harvesting [43]. As a result, it is unnecessary to carefully set up and calibrate the system. This study further suggests that VR applications involving motion tracking may be feasible because when the solar cell is attached to the hand, it may appear at different angles within the line of sight of the laser.

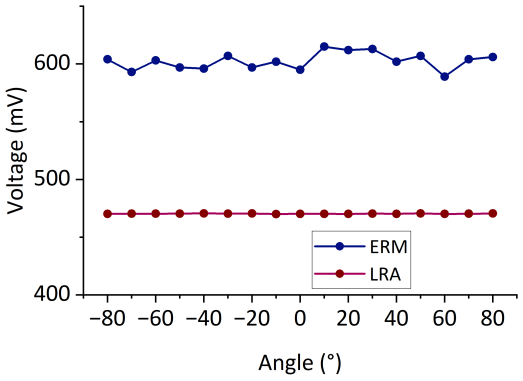

Fig. 4. Voltage output of the ERM motor and LRA (Vrms) with different angles of incidence of the laser.

5.3 How Does Laser Power Level Impact Output Power And Vibration Intensity?

This study investigated the impact of varying laser power levels on the output power of the PV cells and the subsequent vibration intensity of the ERM motor and LRA. The experiment setup was similar to the first study. The size of the laser beam was adjusted to approximately $368cm^2$ to cover the combined area of the two PV cells, by positioning the laser source at a distance of 5m away from the cells. The effect of laser power at different levels was assessed by varying the power of the laser from 227mW to 600mW for the ERM motor motor and 50mW to 600mW for the LRA. The lower boundary of 227mW was selected for the ERM motor motor because it generates an output of 350mW on the PV cells, which is the minimum power required to actuate the ERM motor. Similarly, the lower boundary of 50mW was selected for the LRA based on the minimum power required to actuate the LRA (35mV VRms on the PV cells). The upper boundary of 600mW ($163mW/cm^2$) was chosen to ensure that the laser power density was lower than the laser-induced damage threshold of $200mW/cm^2$.

The intensity of vibration was measured using an ADXL335 accelerometer attached to the motor. The analog signal was collected using Analog Discovery 2 [11]. The voltage peak-to-peak (Vpp) was recorded to demonstrate the intensity of vibration, as the acceleration exhibited a sine wave pattern. To reduce the rise time and initiate the vibration of the ERM motor under low power input, we introduced an overdrive voltage generated using a 500mW laser beam with a duration of 10ms.

Results. Our result revealed interesting trends between the output voltage and vibration intensity (Figure 5a-b). For the ERM motor, the output power exhibits a swift rise until the laser power reaches 400mW, beyond which the rate of increase levels off. Notably, increasing the laser power from 500mW to 600mW did not result in an increase in output power, as the PV cells had already reached their maximum output voltage of 1310mV. Of particular interest is the observation that subtle variations in laser power at low levels may result in significant changes in vibration intensity. This has important implications for generating rich vibrotactile patterns, such as progressive increases or decreases in intensity.

In the LRA condition, the output power of the PV cells showcases a different pattern, especially in the range of 500-600mW, wherein a continued increase in output power is observed with the increase in laser power. Despite this rise, there is no corresponding increase in the vibration intensity (Figure 5b). This can be attributed to the LRA reaching its threshold of maximum vibration intensity at around 512mW. These findings suggest that a 500mW laser would be optimal for achieving a balance between laser power strength and vibration intensity for both ERM and LRA in our specific implementation.

Lastly, our PV cell showed a relatively low conversion rate ranging from 2.7% to 8.3% for the ERM motor and 0.06% to 8.9% for the LRA (Figure 5c), suggesting the potential for elevated output power through higher-end solar cells. In the ERM motor condition, there's an inflection point in the conversion rate, indicating that beyond a laser power of 400mW, the output power of the PV cells has a diminishing rate of increase, again, due to the PV cells reaching their maximum output voltage.

5.4 Evaluation of PV Cell Output with Fixed Resistor

To further validate the findings presented in Section 5.3, we conducted another study to assess the output power and voltage of PV cells when a fixed resistor was introduced. This study aimed to investigate the effects of laser power on the output of the PV cells under a DC signal condition. To closely resemble the conditions in Section 5.3, a resistance value of 47 Ohms, which closely approximates the resistance of the ERM motor utilized in that section, was selected. Similar to the method employed in Section 5.3, a range of laser powers, spanning from 227mW to 600mW with an increment of 100mW, were tested. It is worth noting that since the power and voltage characteristics ($P = UI$) of the resistor remain consistent for both DC and AC signals, we expected that the insights gained from the DC condition could be generalized to the AC condition. Therefore, we did not conduct a separate study for the AC condition.

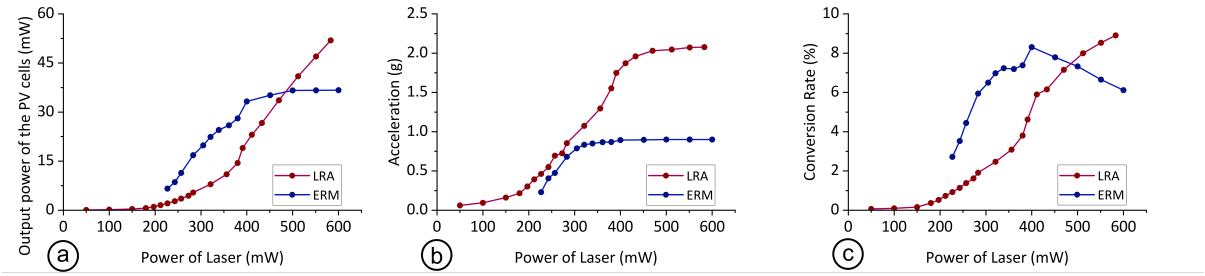

Fig. 5. (a) Output power of the PV cells shown by different laser power levels. (b) Acceleration of the ERM motor and LRA shown by different laser power levels (c) Conversion Rate of the ERM motor and LRA shown by different laser power levels

Results. As shown in Figure 6, the output power and DC voltage of the PV cell demonstrate a rapid increase until the laser power reaches approximately 400mW. Beyond this threshold, the rate of increase stabilizes. It is worth noting that this observation aligns with the results obtained from the previous study that utilized an ERM motor.

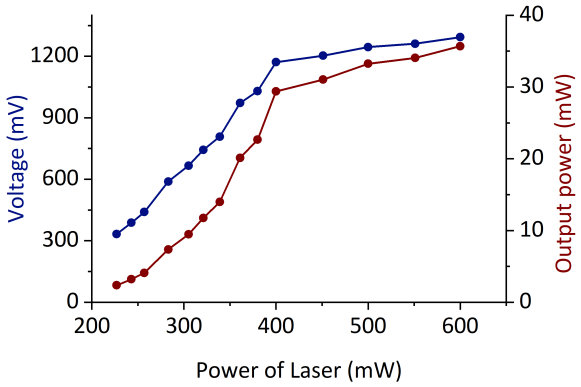

Fig. 6. Voltage and output power of the PV cells with a fixed resistor shown by different laser power levels

5.5 Effectiveness of Overdrive Voltage

This study aims to assess the effectiveness of our overdrive implementation in expediting the rise time of the ERM motor. The overdrive was implemented by introducing a 10ms 500mW laser (1310mV output) as a prefix for three laser power levels, including 335mW, 361mW, and 391mW, which resulted in corresponding outputs of 1015mV, 1100mV, and 1216mV. The rise time of the ERM motor was determined by analyzing the accelerometer data. The Analog Discovery 2 was used to collect the analog signal from the ERM circuit.

Results. Figure 7 shows the effectiveness of overdrive in reducing the rise time of vibrations. Specifically, the application of overdrive resulted in an average reduction of 9.93% in the rise time. As expected, the influence of overdrive on reducing the rise time was found to be more pronounced in the lasers with lower power.

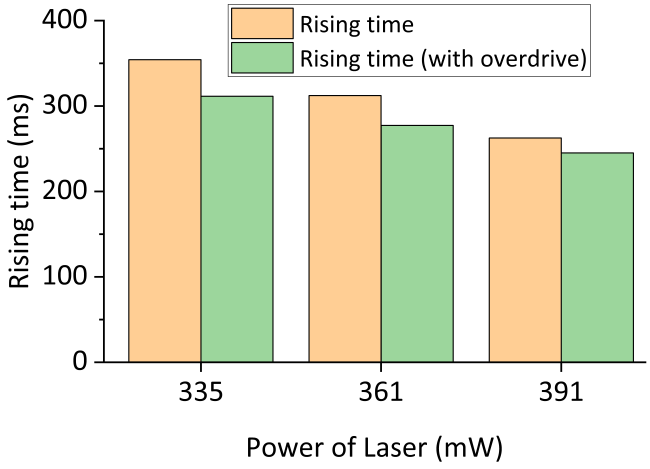

Fig. 7. Rise time with and without overdrive shown by different laser power levels.

6 VIBROTACTILE PATTERNS

To demonstrate the potential of our system, we implemented 16 vibration patterns for both the ERM motor and LRA, among which, 9 were created using a single motor, while the other 7 patterns were created using two motors. The latter set of patterns consisted of 4 alternating patterns and 3 concurrent patterns. The selected patterns are representative of widely used patterns in both industrial and academic settings [23]. Figure 8 and Figure 9 illustrate some of the implemented patterns and their corresponding signals. Most of the selected patterns are compounding patterns, which are combinations of two or three simpler patterns. For the sake of conciseness, we do not present the simpler patterns individually to avoid redundancy. It is worth noting that the resulting pattern shapes and vibration indensities, as detected using an accelerometer, are not identical between our LRA and ERM implementations, particularly in the case of dual motor control. This is due to the reduced duty cycle and longer rising and braking time of the ERM motor when compared to the LRA.

6.1 Single Motor Vibration Patterns

We implemented nine distinct patterns using a single actuator, employing varying levels of vibration intensity and duration.

Single/Double/Triple Click (No.1-3). Single Click displays a 100ms vibration measured at a PTP acceleration of $1.2m/s^2$ (500mW laser) using the ERM motor and $1.85m/s^2$ (420mW laser) using the LRA. Double Click and Triple Click exhibit the occurrence of two and three Single Clicks, separated by a short interval of 100ms.

Buzz (No.4). A 100ms vibration exhibiting a PTP acceleration of $1.2m/s^2$ for the ERM and $1.5m/s^2$ for the LRA, produced by a laser of 500mW for the ERM and 360mW for the LRA, with a brief interval of 100ms.

*Intense-Subtle (No.5).*A 150ms intense vibration measured at a PTP acceleration of $1.8m/s^2$ (500mW laser) for the ERM and $1.85/s^2$ (400mW laser) for the LRA, followed by a 50ms subtle vibration measured at a PTP acceleration of $0.8m/s^2$ (500mW laser) for the ERM motor and $0.32m/s^2$ (200mW laser) for the LRA. Notably, the ERM motors require higher PTP acceleration for short-period vibration to provide a clear vibrotactile feedback.

Intense-Subtle-Subtle (No.6). Similar to Intense-Subtle except for the presence of two instances of the subtle vibratory stimulus.

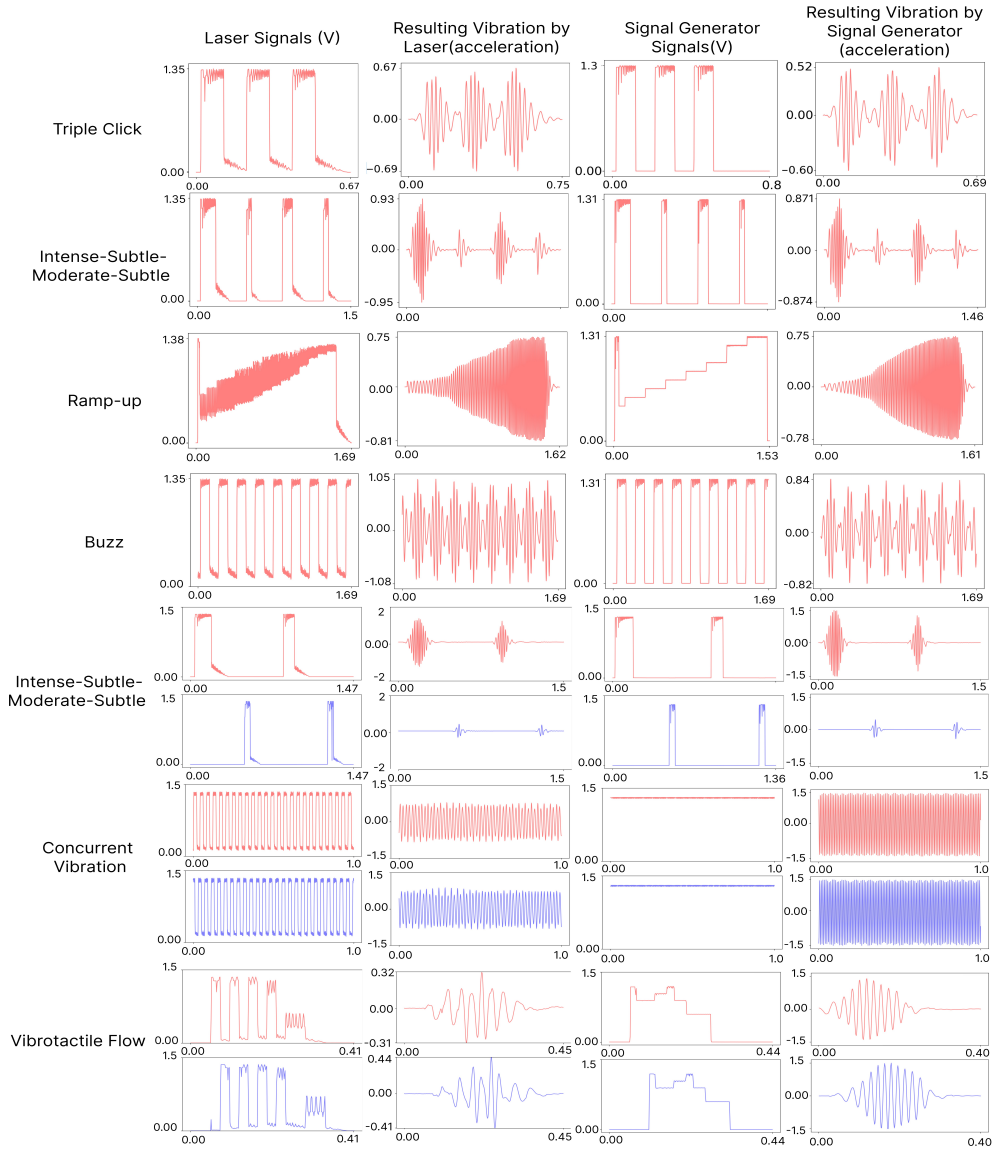

Fig. 8. Illustration of representative vibrotactile patterns developed using a single (Red Line) and two ERM motors (Red and Blue Lines), shown by the laser signals created to generate the target patterns (col. 1), the corresponding resulting patterns generated by the laser (col. 2), the signal generator signals created to generate the target patterns (col. 3), and the corresponding resulting patterns generated by the signal generator (col. 4).

Intense-Subtle-Moderate-Subtle (No.7). A sequential presentation of two Intense-Subtle with the second intense vibration rendered 2 times weaker than the initial presentation using a 100ms 500mW for the ERM and 100ms 350mW laser for the LRA.

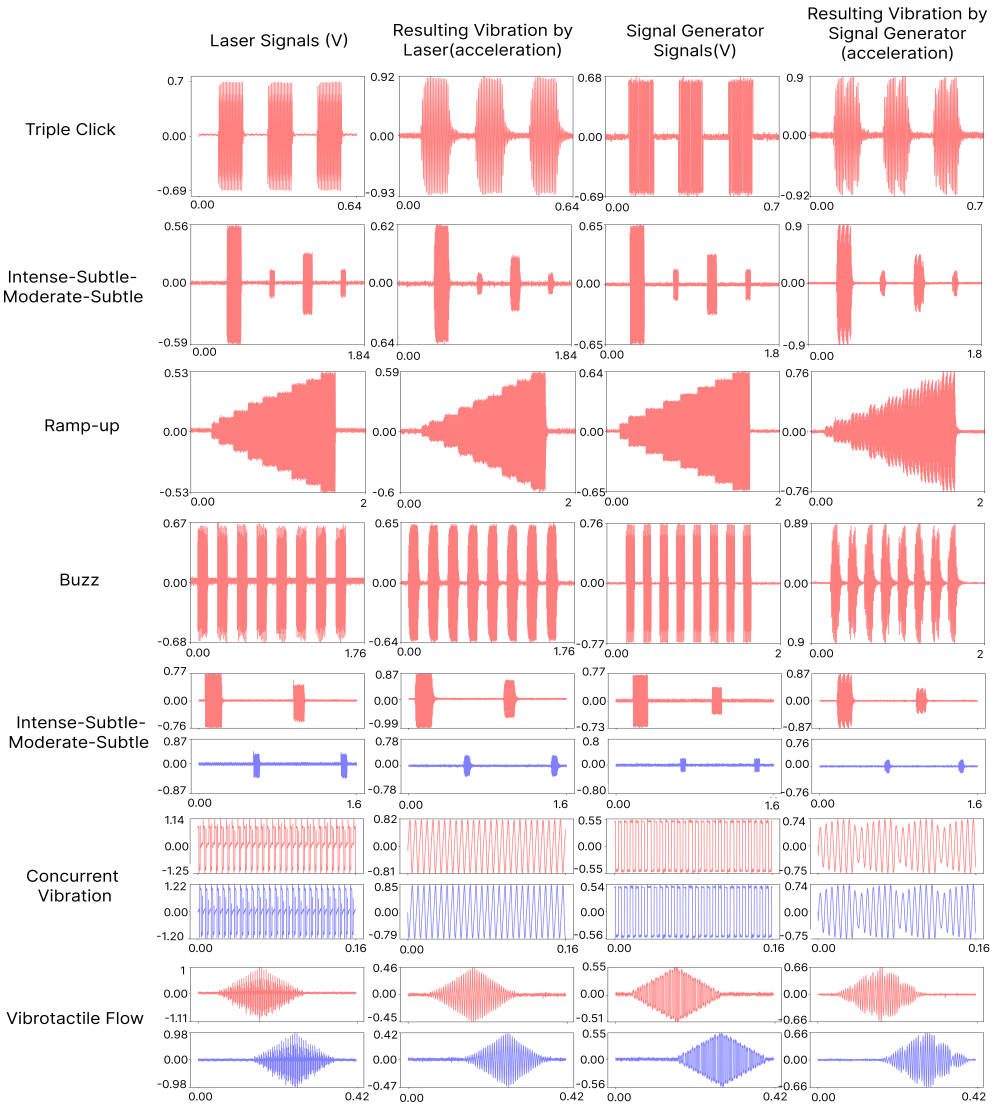

Fig. 9. Illustration of representative vibrotactile patterns developed using a single (Red Line) and two ERM motors (Red and Blue Lines), shown by the laser signals created to generate the target patterns (col. 1), the corresponding resulting patterns generated by the laser (col. 2), the signal generator signals created to generate the target patterns (col. 3), and the corresponding resulting patterns generated by the signal generator (col. 4) (the fluctuations caused by the signal generator are hardly perceivable by a human)

Ramp-Up (No.8). The vibration intensity exhibits an incremental rise (9 steps) from an initial value of $0.2m/s^2$ to a final value of $1.6m/s^2$ for the ERM and from $0.2m/s^2$ to $1.3m/s^2$ for the LRA over a 1.6s duration. The highest intensity was achieved through the laser operating at 433mW for the ERM and 350mW for LRA, while the lowest

intensity was produced with the laser operating at 227mW for the ERM and 180mW for the LRA. We used an overdrive at the beginning to initiate the vibration for the ERM motor.

Ramp-Down (No.9). Ramp-Down is the opposite of Ramp-Up, whereby the vibration intensity progressively reduces. The highest intensity was achieved through the laser operating at 500mW for the ERM and 350mW for the LRA, while the lowest intensity was generated with the laser operating at 257mW for the ERM and 180mW for the LRA.

6.2 Alternating Patterns with Two Motors

We made slight adjustments to the vibration patterns developed for a single motor and generated four additional patterns by incorporating alternating vibrations between two motors. Implementation of these patterns was achieved through the use of a single laser source as described early.

Intense-Subtle-Alt (No.10). Following an intense vibration on a motor, a subtle vibration is rendered on a different motor.

Intense-Subtle-Subtle-Alt (No.11). Subsequent to the intense vibration on a motor, two subtle vibrations were rendered on a different motor.

Intense-Subtle-Moderate-Subtle-Alt (No.12). The order remains the same as the single motor version, except for the allocation of high/moderate and subtle vibrations, which were rendered on separate motors as opposed to a singular motor.

Buzz-Alt (No.13). The rendering of buzzing alternates between the two motors.

6.3 Concurrent Patterns with Two Motors

We implemented three concurrent vibration patterns by incorporating the simultaneous operation of two motors using a single laser source. As described in the previous section, the concurrent operation of the motors with a single laser source leads to a reduction in the maximum vibration intensity by half.

SingleClick-Buzz (No.14). It renders the Single Click on one motor and Buzz concurrently on the other motor.

Buzz-Buzz (No.15). It renders Buzz concurrently on both motors.

Vibrotactile Flow (No.16). Vibrotactile Flow induces a sense of a moving object between two motors[42]. This was implemented by presenting two overlapping sets of ramp-up-and-down patterns, one on each motor (Figure 9; Row 7, Column 3).

For the ERM, however, the challenge is that our ramp-up implementation developed on a single motor could not be used for simultaneous control, especially at the beginning of the ramp, where the vibration intensity is low. This was due to the deceleration of the motor once the laser was moved away from its PV cells, making it difficult for the motor to reach the desired speed. To address this challenge, we used a laser with a higher power (500mW in our implementation). This allowed the motor to accelerate faster than it decelerated, an important requirement for increasing vibration intensity in simultaneous control where each motor is allocated an equal share of 50% duty cycle. We set the duty cycle to 23ms, which resulted in a steady increase in vibration intensity from a PTP acceleration of approximately $0.3m/s^2$ to $0.8m/s^2$ in 115ms (3 cycles as shown in Figure 8). Ramp-down does not have this problem. In our implementation, the reduction of vibration intensity was achieved by progressively decreasing the laser power from 500mW to 391mW, and subsequently to 212mW, resulting in a PTP acceleration of $0.3m/s^2$.

The LRA does not have the same issue. Thus, we could use the same method developed for a singular actuator to achieve both ramp-up and ramp-down. In our implementation, the highest intensity of $1.1m/s^2$ was achieved through the laser operating at 370mW, whereas the lowest intensity of $0.15m/s^2$ was achieved using a 180mW laser.

As with other vibrotactile flow generated using vibratory stimuli [54], we enhance users' perceptual experience by incorporating visual feedback of a rolling ball (Figure 10, right).

7 USER STUDY

We conducted a user study to evaluate the subjective assessment of users' initial exposure to the vibrotactile patterns generated by our approach. Our study task involved exposing participants to a range of vibrotactile patterns applied to their hand, simulating what is typically encountered in a VR environment. Our choice of task was motivated by the fact that VR applications impose higher demands for high-quality haptic rendering compared to other use cases of our device.

We would like to note that, generally speaking, LRAs are capable of producing more noticeable and immediate changes in vibration compared to ERM motors. This is mainly due to their unique characteristics, such as shorter starting and braking times and lower power requirements to initiate vibrations. Therefore, delivering the designed patterns with high quality using ERM motors presents a more significant challenge compared to LRAs (as confirmed by our pilot study). In this study, we deliberately focused on ERM motors, which enabled us to gain insights into the lower limit of our approach. Additionally, we were interested in understanding how our approach would perform in comparison to those relying on electronics. Thus, we included a baseline condition with the same set of patterns generated using a signal generator. Although we could have implemented the baseline through a microcontroller and driver, we chose the signal generator to generate analog signals, which are generally more optimal for motor control.

7.1 Participants and Apparatus

Seven right-handed participants (2 females and 5 males) were recruited to participate in the study. Although the sample size was relatively small, it conforms to the common practices in haptics research of similar studies [5, 13, 40]. During the study, a pair of ERM motors were affixed to the palm of the dominant hand of each participant with a distance of 30mm and 50mm for female and male participants, respectively (Figure 10, left). In order to generate the concurrent patterns in the baseline condition, two signal generators were used, with each of them controlling a separate motor, whereas our method utilized a single laser source operating at 500mW.

To ensure a fair comparison between the two methods, the maximum voltage output of the signal generator was limited to 1.3V, which corresponds to the maximum voltage output of our prototype for the ERM motor. Additionally, we ensured that salient features of the tested vibrotactile patterns, such as vibration intensity and duration, remained the same across both implementation methods.

While our implementation is, in principle, deemed safe for human body application, laser-based technologies, by their nature, necessitate a more careful study design to ensure participant safety, particularly during the technology's early developmental phase. Consequently, we have opted for a more stringent IRB protocol to strategically partition the laser component from direct participant interaction, thus minimizing potential risks during the course of our study. Specifically, the laser and solar cells were situated within a protected laser operation space covered with safety curtains. The distance between the laser and PV cells was set at 5 meters (Figure. 11). The participants were seated in an adjacent room. They were advised to maintain a relaxed posture of their choice while completing the study. The experimental interface was presented on a 27-inch monitor placed on a desk in front of the participants.

7.2 Task and Procedure

The study consisted of two sessions, which were presented to the participants in a randomized order. During Session A, participants were presented with all the vibration patterns as detailed in the previous section, with the exception of Vibrotactile Flow, which was assessed in Session B due to its unique requirements for visual feedback.

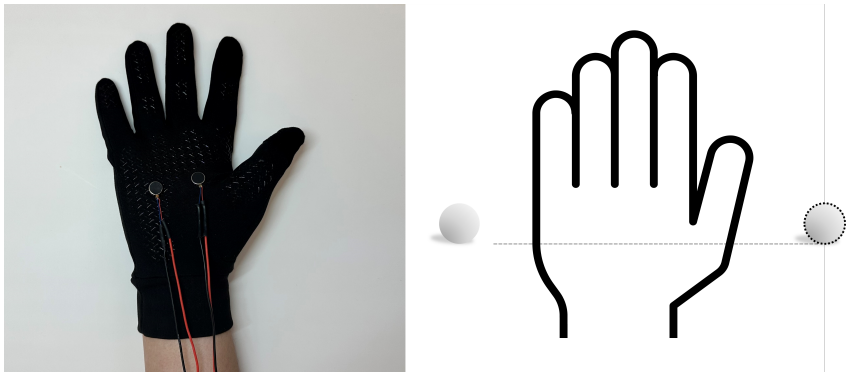

Fig. 10. Left: Participant's right hand wearing a glove with two ERM motors. Right: In the Vibrotactile Flow condition, we showed the visual feedback of a rolling ball moving in and out on a participant's hand from left to right.

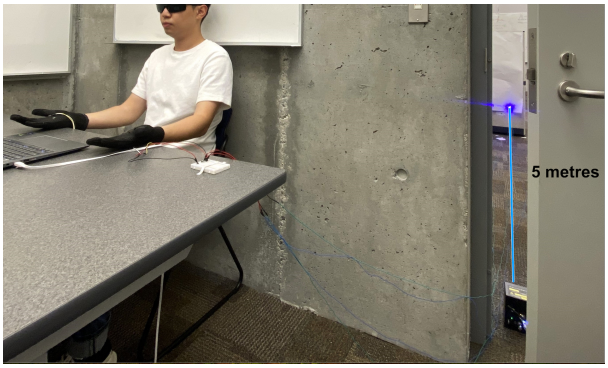

Fig. 11. The setup of our study.

The method of delivery, either through the laser or signal generator was randomly assigned. Since the vibration patterns using one or two motors could be easily differentiated, we chose to present them as two separate groups, and in a randomized order. Following the presentation of each vibration pattern in Session A, participants were required to select a text description from a pre-determined list that most accurately described the pattern they perceived. Additionally, they were instructed to provide a continuous numerical rating to evaluate the degree of congruence between the selected text description and the presented vibration pattern (1 being a complete mismatch and 5 being a perfect match).

The evaluation of Vibrotactile Flow was conducted during Session B, as it was paired with a visual display of a rolling ball (Figure 10, right). The tactile experience was activated upon the virtual ball crossing the virtual line on the left, emulating its entry from the left side of the hand and subsequent exit from the right. The vibrotactile feedback was terminated once the virtual ball crossed the virtual line on the right. Following the presentation of the Vibrotactile Flow produced by either the laser or the signal generator, the participants were asked to provide a continuous numerical rating to assess the degree of realism.

Before the study, participants were given a brief introductory session to acquaint them with the experimental apparatus. No specific training was provided to familiarize them with the tested vibration patterns. Our pilot study findings indicate that the recognition of vibration patterns, particularly those involving subtle vibrations,

Table 1. The average and standard deviation of the congruence scores collected from our user study.

	No.1	No.2	No.3	No.4	No.5	No.6	No.7	No.8
Laser: Average	5	4.86	5	4.64	4.2	4.56	4.08	4.64
Laser: STD	0	0.38	0	0.75	0.84	0.88	0.92	0.63
Analog: Average	5	5	5	4.86	4.03	4.41	4.67	4.79
Analog: STD	0	0	0	0.37	0.9	0.92	0.52	0.4
	No.9	No.10	No.11	No.12	No.13	No.14	No.15	No.16
Laser: Average	4.07	4.43	5	4.71	4.71	4.57	4.14	4.29
Laser: STD	0.84	0.98	0	0.76	0.49	1.13	0.9	0.76
Analog: Average	4.57	4.29	5	5	4.86	4.79	4.29	4.14
Analog: STD	0.53	0.95	0	0	0.38	0.39	0.95	0.69

improves with repeated exposure. To gauge the initial reactions of the participants, we restricted their exposure to each pattern to a single trial.

7.3 Results and Discussion

Figure 12 shows confusion matrices that illustrate the recognition accuracy of the tested vibrotactile patterns rendered via the laser and the baseline. The degree of congruence is shown in Figure 13.

The participants in the study did not report any noticeable differences between the laser and baseline conditions, as indicated by the congruence scores presented in Table 1. To further explore this finding, we conducted a paired-sample t-test for all the patterns, with the exception of the Click, Triple Click, and Vibration-Vibration patterns, which all received a full score of 5. Additionally, data points where participants failed to correctly recognize a pattern were excluded from the analysis, resulting in the removal of 7 out of 224 data points (3.1%). The results of the analysis revealed that all the p-values were greater than 0.05, indicating that no statistically significant differences in means between conditions were observed. Although conducting the study with a larger number of participants may potentially reveal a statistically significant difference, the current results suggest that any numerical difference would likely be small. In fact, all participants commented that the vibrations felt identical to them under both conditions.

The participants were able to accurately recognize the majority of the vibration patterns, regardless of the power source driving the motors. The results also revealed a consistent pattern concerning the recognition accuracy across the laser and baseline conditions. Specifically, those with low recognition accuracy remained consistently low irrespective of the power source, while those with high accuracy remained consistently high for both methods. These results suggest that laser-powered vibrotactile rendering has the potential to replace electronic systems with comparable performance.

The majority of the recognition errors were associated with patterns containing subtle vibrations, which subsequently resulted in lower ratings as the participants found them difficult to perceive. Analysis of the participants' feedback identified three primary reasons contributing to the errors, namely, failure to detect the subtle vibrations, misconstruing them as motor noise, or misperceiving them as intense vibrations. Notably, all of them are linked to the perception of subtle vibrations. The participants emphasized that these errors could have been avoided if they were given further trials or changed their previous results. The common mistakes made by the participants include recognizing Intense-Subtle or Intense-Subtle-Subtle as Single Click or Triple Click (P3, P5), Intense-Subtle-Moderate-Subtle as Intense-Subtle (P3).

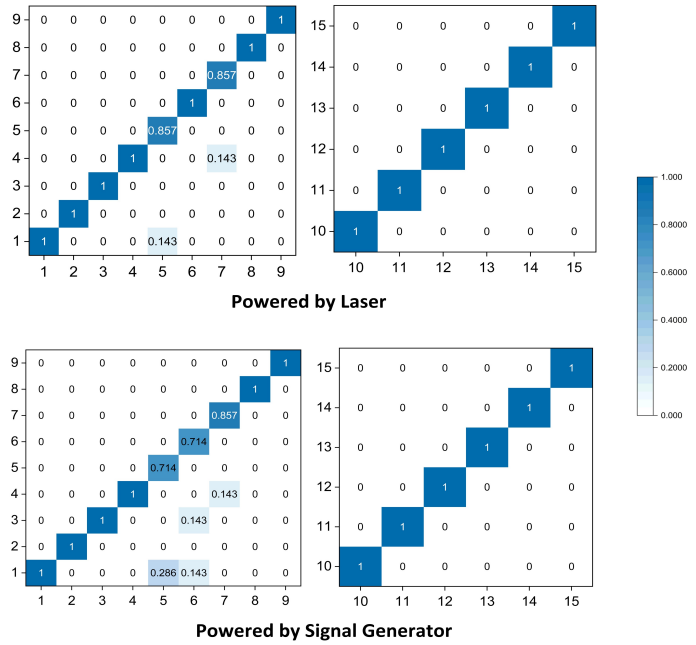

Number	Vibrotactile Patterns
No.1	Click
No.2	Double Click
No.3	Triple Click
No.4	Buzz
No.5	Intense-Subtle
No.6	Intense-Subtle-Subtle
No.7	Intense-Subtle-Moderate-Subtle
No.8	Ramp-Up
No.9	Ramp-Down
No.10	Intense-Subtle-Alt
No.11	Intense-Subtle-Subtle-Alt
No.12	Intense-Subtle-Moderate-Subtle-Alt
No.13	Buzz-Alt
No.14	SingleClick-Buzz
No.15	Buzz-Buzz
No.16	Vibrotactile Flow

Fig. 12. The confusion Matrices of the vibrotactile patterns rendered using the ERM motor(s)

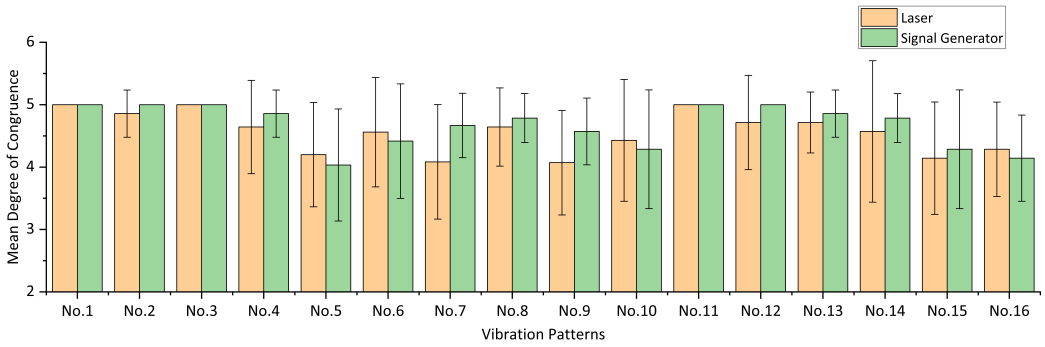

Fig. 13. Mean Degree of Congruence shown by the powering methods and 16 tested patterns (SD = 1).

7.4 Vibrotactile Flow

The results indicated an average rating of 4.29 and 4.14 for the laser and baseline condition, respectively (Pattern 16 in Figure 13). A t-test revealed no statistically significant difference between the two methods ($p = 0.356$). The results again suggest that the laser-powered vibrotactile rendering method yields comparable performance to the baseline approach using a signal generator. Notably, the results are particularly encouraging as the baseline condition involved the use of two signal generators, while only one laser source was used to drive two motors in the laser condition.

8 ENVISIONED APPLICATIONS

To demonstrate the versatility of our approach, we present a diverse set of use cases that leverage our device to facilitate novel haptic interactions. In Figure 14 we present a detailed depiction of our entire system, including a proposed tracking system that we envision integrating in the future. Our applications are classified into three categories (1) battery-free haptic gloves, (2) ambient haptic feedback, and (3) adaptation of conventional input devices.

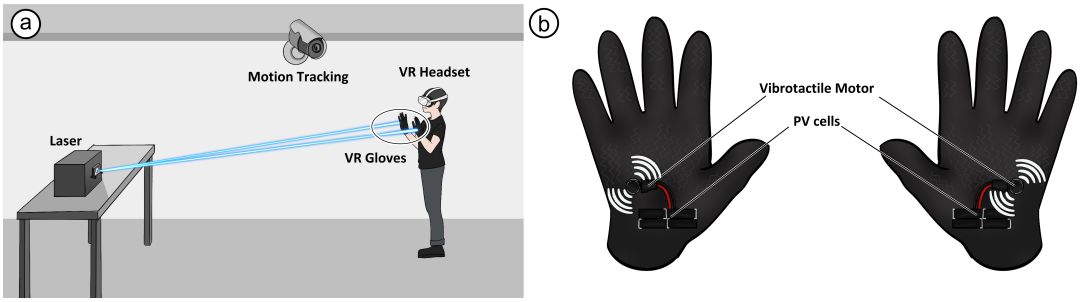

Fig. 14. (a) A hypothetical utilization of our system in VR applications. The system is comprised of various components, including a laser, a motion tracking system (to be incorporated in the future), a VR headset, and our haptic gloves. (b) Details of the haptic gloves comprising PV cells and vibrotactile motors.

8.1 Battery-Free Haptic Gloves

We implemented a pair of haptic gloves with two LRAs strategically attached to the palm of each glove. These LRAs were then tethered to the PV cells affixed to the lag of the table placed in front of the user. This design choice allows the user to freely move their hands without the tangling of wires. To showcase the capability of our device, we developed two VR demo applications (Figure 15). In the first demo, users are presented with the realistic sensation of a butterfly landing on their hand. In the second demo, we implemented the vibrotactile flow [42] by enabling users to perceive the sensation of a spider crawling across their palm from left to right. Unlike the existing approaches, our system features an extended operational time, thus obviating the need for frequent charging.

8.2 Ambient Haptic Feedback

Ambient haptic interfaces aim to seamlessly integrate haptic feedback into everyday environments, providing unobtrusive access to haptic experiences in home or work settings. The challenge with current approaches is the need for battery replacement and recharging of haptic devices. Our proposed device could facilitate the easy deployment of ambient haptic interfaces in everyday environments. For example, we present a door handle of a meeting room augmented with our device that vibrates when touched, indicating that the room is in use by someone (see Figure 1b). Additionally, we illustrate how our device can be attached to a sofa, which vibrates to remind the user of an upcoming important meeting appointment (see Figure 1d). As a new way to enable ambient haptics, our approach has the potential to minimize the inconvenience associated with charging and replacing batteries in haptic devices.

8.3 Adaptation of Conventional Input Devices

In the third scenario, we demonstrate the potential of the proposed device to enhance conventional input devices, such as mice or keyboards, designed for prolonged use. As the contemporary usage of such devices has expanded

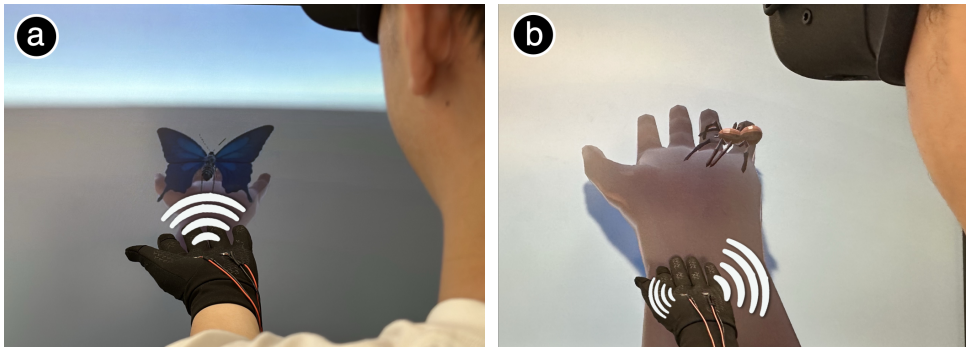

Fig. 15. Eenvisioned applications of our proposed device in VR environments. (a) A user feels a butterfly landing on their hand. (b) A user feels a spider crawling across their palm. This demo was developed using our implementation of Vibrotactile Flow.

to encompass activities that necessitate more sophisticated haptic feedback, such as gaming, there is a growing need for more immersive haptic experiences in these scenarios. However, a significant challenge faced is the limited battery life associated with integrating a vibration motor. Our proposed device could be a temporary attachment to a computer mouse (with PV cells affixed to the lag of the table) that offers users the ability to experience haptic impulses when simulating the firing of a gun or the tactile edge of virtual objects during the alignment of shapes or objects using the cursor.

9 LIMITATIONS AND FUTURE WORK

In this section, we present the observations and insights garnered throughout the course of our research. Additionally, we discuss the limitations of our work and outline a plan for future investigations.

Conversion efficiency. Despite the relatively low conversion rate of 10% observed in our current implementation, our research effectively demonstrated the potential of utilizing laser to energize and control both LRA and ERM motors, enabling them to provide haptic feedback across various vibration intensities. However, further exploration is necessary to fully exploit the capabilities of our approach. One avenue for improvement lies in leveraging high-efficiency solar cells, specifically, those composed of Gallium arsenide, which have exhibited efficiencies exceeding 30%. Another potential strategy to enhance the conversion efficiency of our system revolves around matching the characteristic resistance of the solar cell. This resistance refers to the output resistance of the cell at its maximum power point. By aligning the resistance of the vibrotactile motor with the characteristic resistance of the solar cell, optimal power transfer to the motor can be achieved, enabling the PV cells to operate at its peak performance. It is important to note that a key distinction between our work and existing studies focusing on efficient circuits tailored for battery-free energy harvesting systems [7, 10] lies in our elimination of all electronics and components on the haptic interface side. This removal significantly reduces the complexity of the hardware user interface, potentially improving the overall user experience.

Laser safety. The power density of our current implementation is similar to that of direct sunlight ($\sim 135 mW/cm^2$), which is sufficient for the operation of LRAs. However, to achieve stronger vibrations using ERM motors, it is possible to increase the power density by raising the laser power or by utilizing solar cells with high conversion efficiency. It is important to note that for safe use of the system with stronger lasers in practical applications, an additional safety mechanism similar to that proposed by Iyer et al. [20] is crucial to ensure prompt termination of laser exposure to the user. Nevertheless, the integration of such a system is beyond the current scope of our research, and we will investigate it in future work.

Distance. During our study, we set the distance between the laser and the PV cell at 5 meters. This distance was chosen to ensure that the laser's power density at the cells remained at a low level of approximately $135 mW/cm^2$. We acknowledge that using a beam expander is a preferable method for controlling the beam size and power density. With a beam expander, the distance constraint is eliminated, and the power density can be maintained at a consistent low level throughout the entire pathway of the beam. However, for the purpose of our initial exploration of this new approach, we opted for the more cost-effective approach of controlling the beam size by adjusting the distance between the laser diode and the cells.

Beyond ERM and LRA. We investigated the feasibility of using laser as a means of powering and controlling LRA and ERM motors. Future research will investigate the compatibility of our approach with other types of actuators, especially those that require high voltage input, such as piezo actuators. Piezo actuators demand approximately 100v AC signals, which poses a challenge to the current approach. However, the energy consumption measurements conducted by Texas Instruments indicate that the power consumption of piezo actuators is comparable to that of ERM motors and LRAs. Specifically, the energy consumption per vibration (or click) is measured as 0.34 uAh for Piezo, 0.58 uAh for LRA, and 1.72 uAh for ERM [17]. These findings suggest that high-voltage PV cells can provide a promising solution to overcome this challenge and improve the versatility of our approach for a broader range of actuators.

Tracking. The accurate delivery of a laser beam to PV cells is a crucial requirement in several target applications. Achieving such precision necessitates the precise tracking of the cells' locations. Tracking the movement of objects in 3D space has been extensively investigated within academia and industry, thus paving a pragmatic path for integrating our proposed method into VR applications. Among the existing tracking methods, a straightforward yet effective approach employs computer vision to track tagged objects [35–37]. Within the context of our work, we envision augmenting the PB cells with retroreflective markers along their periphery. The 3D position of the markers can subsequently be tracked using a camera and established computer vision techniques, resulting in millimeter-level precision [38] with latency at the millisecond scale [37]. This latency remains imperceptible to human perception [24].

The speed of the galvo plays an equally important role in guaranteeing precise laser beam delivery. Considering that the fastest human motion at around 44 m/s [20] – translating to angular velocities of 44 rad/s, 8.8 rad/s, and 4.4 rad/s when the laser is positioned 1 m, 5 m, and 10 m away from the PV cell, respectively. Note that the commonly used galvo scanners in commercial products can significantly surpass these angular velocities. For instance, our current implementation uses a galvo system with an angular velocity of approximately 4,221 rad/s, outpacing human motion by 480 times at a 5 m distance from the laser. Our upcoming research will investigate suitable tracking methods that can enable untethered solutions.

In addition, we will also seek to determine the maximum number of vibration motors that can be controlled by a single laser source and develop an optimal control algorithm that can handle multiple moving cells within a room.

Sensing user input. The present implementation lacks the ability to perceive the user's input during the interaction with physical objects augmented with ambient haptic feedback. Our forthcoming research will investigate methods for repurposing the existing approach and laser system to facilitate user input detection while minimizing the usage of additional devices on the laser side. We see that a potential avenue for achieving this objective is through laser speckle imaging techniques [4].

Sensing vibration frequency. Our current implementation lacks the ability to detect the vibration frequency of the motor, posing a challenge in achieving accurate and timely vibrotactile rendering. To address this limitation, we plan to explore approaches to repurpose the laser for sensing the motor's vibration frequency. This adaptation would enable the system to establish a closed loop, facilitating real-time adjustments to the motor's output based on sensor feedback. Consequently, this enhancement will provide us with finer-grained control over how vibrotactile experiences can be precisely rendered. A potential solution for achieving non-contact vibration

sensing could draw inspiration from the methods often utilized in laser Doppler vibrometers [53]. Additionally, tracking the motor's location can be accomplished using computer vision methods, as discussed earlier.

10 CONCLUSION

This paper presents a battery-free and electronic-free vibrotactile device that leverages a laser-based wireless power transfer and haptic control mechanism. The proposed solution enables the driving of vibrotactile motors using both DC and AC signals. Through the development of a proof-of-concept prototype and a series of technical evaluations and user studies, we demonstrate the feasibility of our approach to replace conventional electronics and batteries in existing devices. The implications of our work extend beyond the domain of vibrotactile devices, offering insights into the advancement of sustainable smart devices in virtual and physical environments. We believe this alternative perspective could foster the growth of sustainable technologies and facilitates the reduction of electronic waste.

REFERENCES

[1] Junjie Bai, Lu Liao, Ying Wu, Yiping Deng, Chengguang Wu, Xiaoyun Zhang, Gang Hu, Yuan Zhai, and Guang Zhu. 2017. A New Type of Self Driven Door Handle. *International Journal of Software Science and Computational Intelligence* 9, 4 (Oct. 2017), 67–79. https://doi.org/10.4018/IJSSCI.2017100105

[2] Surajit Das Barman, Ahmed Wasif Reza, Narendra Kumar, Md. Ershadul Karim, and Abu Bakar Munir. 2015. Wireless powering by magnetic resonant coupling: Recent trends in wireless power transfer system and its applications. *Renewable and Sustainable Energy Reviews* 51 (2015), 1525–1552. https://doi.org/10.1016/j.rser.2015.07.031

[3] bHaptics. 2023. Next generation full body haptic suit - bHaptics TactSuit. Retrieved May 15, 2023 from https://www.bhaptics.com/

[4] Silvio Bianchi. 2014. Vibration detection by observation of speckle patterns. *Applied optics* 53, 5 (2014), 931–936. https://doi.org/10.1364/AO.53.000931

[5] Cristiano Carvalheiro, Rui Nóbrega, Hugo da Silva, and Rui Rodrigues. 2016. User Redirection and Direct Haptics in Virtual Environments. In *Proceedings of the 24th ACM International Conference on Multimedia* (Amsterdam, The Netherlands) *(MM '16)*. Association for Computing Machinery, New York, NY, USA, 1146–1155. https://doi.org/10.1145/2964284.2964293

[6] Qi Chen, Dechen Zhang, Dandi Zhu, Qianyun Shi, Jian Gu, and Yong Ai. 2015. Design and experiment for realization of laser wireless power transmission for small unmanned aerial vehicles. In *AOPC 2015: Advances in Laser Technology and Applications*, Vol. 9671. SPIE, 133–139. https://doi.org/10.1117/12.2199235

[7] Alexei Colin, Emily Ruppel, and Brandon Lucia. 2018. A reconfigurable energy storage architecture for energy-harvesting devices. In *Proceedings of the Twenty-Third International Conference on Architectural Support for Programming Languages and Operating Systems*. 767–781.

[8] Jasper de Winkel, Vito Kortbeek, Josiah Hester, and Przemysław Pawełczak. 2020. Battery-Free Game Boy. *Proceedings of the ACM on Interactive, Mobile, Wearable and Ubiquitous Technologies* 4, 3 (Sept. 2020), 111:1–111:34. https://doi.org/10.1145/3411839

[9] Alexandra Delazio, Ken Nakagaki, Roberta L. Klatzky, Scott E. Hudson, Jill Fain Lehman, and Alanson P. Sample. 2018. Force Jacket: Pneumatically-Actuated Jacket for Embodied Haptic Experiences. In *Proceedings of the 2018 CHI Conference on Human Factors in Computing Systems (CHI '18)*. Association for Computing Machinery, New York, NY, USA, 1–12. https://doi.org/10.1145/3173574.3173894

[10] Harsh Desai, Matteo Nardello, Davide Brunelli, and Brandon Lucia. 2022. Camaroptera: A long-range image sensor with local inference for remote sensing applications. *ACM Transactions on Embedded Computing Systems (TECS)* 21, 3 (2022), 1–25.

[11] Digilent. 2023. *Analog Discovery 2: 100MS/s USB Oscilloscope, Logic Analyzer and Variable Power Supply*. Retrieved May 15, 2023 from https://digilent.com/shop/analog-discovery-2-100ms-s-usb-oscilloscope-logic-analyzer-and-variable-power-supply/

[12] Engadget. 2019. Sony envisions 'clothes' with haptic feedback for PSVR. Retrieved May 15, 2023 from https://www.engadget.com/2019-05-23-sony-ps5-vr-gloves-patent-haptic-feedback-bodysuit.html

[13] Cathy Mengying Fang and Chris Harrison. 2021. Retargeted Self-Haptics for Increased Immersion in VR without Instrumentation. In *The 34th Annual ACM Symposium on User Interface Software and Technology* (Virtual Event, USA) *(UIST '21)*. Association for Computing Machinery, New York, NY, USA, 1109–1121. https://doi.org/10.1145/3472749.3474810

[14] Taku Hachisu, Sayaka Oshima, Yuki Hashimoto, and Hiroyuki Kajimoto. 2010. Haptic illusion of elasticity by tactile suppression during motor activity. In *2010 IEEE Haptics Symposium*. 55–58. https://doi.org/10.1109/HAPTIC.2010.5444678

[15] Seongkook Heo, Jaeyeon Lee, and Daniel Wigdor. 2019. PseudoBend: Producing Haptic Illusions of Stretching, Bending, and Twisting Using Grain Vibrations. In *Proceedings of the 32nd Annual ACM Symposium on User Interface Software and Technology (UIST '19)*. Association for Computing Machinery, New York, NY, USA, 803–813. https://doi.org/10.1145/3332165.3347941

[16] American National Standards Institute and Laser Institute of America. 2022. *ANSI A136.1-2022 American National Standard for Safe Use of Lasers*. The Laser Institute of America, Orlando, FLa, USA.
[17] Texas Instruments. 2022. *Application Note: Haptic Energy Consumption*. Technical Report. Dallas, Texas, USA. https://doi.org/lit/an/sloa194a/sloa194a.pdf?ts=1684114802202&ref_url
[18] Texas Instruments. 2023. *DRV2605*.
[19] Md Shafiqul Islam and Sol Lim. 2022. Vibrotactile feedback in virtual motor learning: A systematic review. *Applied Ergonomics* 101 (May 2022), 103694. https://doi.org/10.1016/j.apergo.2022.103694
[20] Vikram Iyer, Elyas Bayati, Rajalakshmi Nandakumar, Arka Majumdar, and Shyamnath Gollakota. 2018. Charging a Smartphone Across a Room Using Lasers. *Proceedings of the ACM on Interactive, Mobile, Wearable and Ubiquitous Technologies* 1, 4 (Jan. 2018), 143:1–143:21. https://doi.org/10.1145/3161163
[21] Johannes James, Vikram Iyer, Yogesh Chukewad, Shyamnath Gollakota, and Sawyer B Fuller. 2018. Liftoff of a 190 mg laser-powered aerial vehicle: The lightest wireless robot to fly. In *2018 IEEE International Conference on Robotics and Automation (ICRA)*. IEEE, 3587–3594.
[22] Jie Jiang and Yue Zhao. 2023. Liquid Crystalline Elastomer for Separate or Collective Sensing and Actuation Functions. *Small* (2023), 2301932. https://doi.org/10.1002/smll.202301932
[23] Francisco Javier Jimenez and J De Frutos. 2005. Virtual instrument for measurement, processing data, and visualization of vibration patterns of piezoelectric devices. *Computer Standards & Interfaces* 27, 6 (2005), 653–663. https://doi.org/10.1016/j.csi.2004.09.010
[24] Ricardo Jota, Albert Ng, Paul Dietz, and Daniel Wigdor. 2013. How Fast is Fast Enough? A Study of the Effects of Latency in Direct-Touch Pointing Tasks. In *Proceedings of the SIGCHI Conference on Human Factors in Computing Systems* (Paris, France) *(CHI '13)*. Association for Computing Machinery, New York, NY, USA, 2291–2300. https://doi.org/10.1145/2470654.2481317
[25] Jae-Hoon Jun, Jong-Rak Park, Sung-Phil Kim, Young Min Bae, Jang-Yeon Park, Hyung-Sik Kim, Seungmoon Choi, Sung Jun Jung, Seung Hwa Park, Dong-Il Yeom, Gu-In Jung, Ji-Sun Kim, and Soon-Cheol Chung. 2015. Laser-induced thermoelastic effects can evoke tactile sensations. *Scientific Reports* 5, 1 (June 2015), 11016. https://doi.org/10.1038/srep11016
[26] Mustafa Emre Karagozler, Ivan Poupyrev, Gary K. Fedder, and Yuri Suzuki. 2013. Paper generators: harvesting energy from touching, rubbing and sliding. In *Proceedings of the 26th annual ACM symposium on User interface software and technology (UIST '13)*. Association for Computing Machinery, New York, NY, USA, 23–30. https://doi.org/10.1145/2501988.2502054
[27] Oliver Beren Kaul and Michael Rohs. 2017. HapticHead: A Spherical Vibrotactile Grid around the Head for 3D Guidance in Virtual and Augmented Reality. In *Proceedings of the 2017 CHI Conference on Human Factors in Computing Systems (CHI '17)*. Association for Computing Machinery, New York, NY, USA, 3729–3740. https://doi.org/10.1145/3025453.3025684
[28] Nobuki Kawashima and Kazuya Takeda. 2008. Laser Energy Transmission for a Wireless Energy Supply to Robots. In *Robotics and Automation in Construction*. IntechOpen. https://doi.org/10.5772/6194
[29] Salman Khan, Jiyong Kim, Somnath Acharya, and Woochul Kim. 2021. Review on the operation of wearable sensors through body heat harvesting based on thermoelectric devices. *Applied Physics Letters* 118, 20 (May 2021), 200501. https://doi.org/10.1063/5.0049347
[30] Jinsoo Kim, Seungjae Oh, Chaeyong Park, and Seungmoon Choi. 2020. Body-Penetrating Tactile Phantom Sensations. In *Proceedings of the 2020 CHI Conference on Human Factors in Computing Systems (CHI '20)*. Association for Computing Machinery, New York, NY, USA, 1–13. https://doi.org/10.1145/3313831.3376619
[31] Geoffrey A. Landis. 1994. Applications for space power by laser transmission. In *Laser Power Beaming*, Vol. 2121. SPIE, 252–255. https://doi.org/10.1117/12.174188
[32] Jianchao Li, Fanghui Yin, Liming Wang, Bin Cui, and Daiming Yang. 2020. Electromagnetic Induction Position Sensor Applied to Anti-Misalignment Wireless Charging for UAVs. *IEEE Sensors Journal* 20, 1 (Jan. 2020), 515–524. https://doi.org/10.1109/JSEN.2019.2940925
[33] Tianxing Li and Xia Zhou. 2018. Battery-Free Eye Tracker on Glasses. In *Proceedings of the 24th Annual International Conference on Mobile Computing and Networking (MobiCom '18)*. Association for Computing Machinery, New York, NY, USA, 67–82. https://doi.org/10.1145/3241539.3241578
[34] J. Lu and Y. Suzuki. 2019. Push-button Kinetic Energy Harvester with Soft-X-ray-charged Folded Multilayer Piezoelectret. *Journal of Physics: Conference Series* 1407, 1 (Nov. 2019), 012021. https://doi.org/10.1088/1742-6596/1407/1/012021
[35] Yuri Mikawa, Tomohiro Sueishi, Yoshihiro Watanabe, and Masatoshi Ishikawa. 2018. Variolight: Hybrid dynamic projection mapping using high-speed projector and optical axis controller. In *SIGGRAPH Asia 2018 Emerging Technologies*. 1–2. https://doi.org/10.1145/3275476.3275481
[36] Yuri Mikawa, Tomohiro Sueishi, Yoshihiro Watanabe, and Masatoshi Ishikawa. 2020. Projection mapping system to a widely dynamic sphere with circumferential markers. In *2020 IEEE International Conference on Multimedia and Expo (ICME)*. IEEE, 1–6. https://doi.org/10.1109/ICME46284.2020.9102813
[37] Yuri Mikawa, Tomohiro Sueishi, Yoshihiro Watanabe, and Masatoshi Ishikawa. 2021. Dynamic Projection Mapping for Robust Sphere Posture Tracking Using Uniform/Biased Circumferential Markers. *IEEE Transactions on Visualization and Computer Graphics* 28, 12 (2021), 4016–4031. https://doi.org/10.1109/TVCG.2021.3111085
[38] Kyriaki Niotaki, Nuno Borges Carvalho, Apostolos Georgiadis, Xiaoqiang Gu, Simon Hemour, Ke Wu, Diogo Matos, Daniel Belo, Ricardo Pereira, Ricardo Figueiredo, Henrique Chaves, Bernardo Mendes, Ricardo Correia, Arnaldo Oliveira, Valentina Palazzi, Federico Alimenti,

Paolo Mezzanotte, Luca Roselli, Francesca Benassi, Alessandra Costanzo, Diego Masotti, Giacomo Paolini, Aline Eid, Jimmy Hester, Manos M. Tentzeris, and Naoki Shinohara. 2023. RF Energy Harvesting and Wireless Power Transfer for Energy Autonomous Wireless Devices and RFIDs. *IEEE Journal of Microwaves* 3, 2 (April 2023), 763–782. https://doi.org/10.1109/JMW.2023.3255581

[39] Yi-Hao Peng, Carolyn Yu, Shi-Hong Liu, Chung-Wei Wang, Paul Taele, Neng-Hao Yu, and Mike Y. Chen. 2020. WalkingVibe: Reducing Virtual Reality Sickness and Improving Realism while Walking in VR using Unobtrusive Head-mounted Vibrotactile Feedback. In *Proceedings of the 2020 CHI Conference on Human Factors in Computing Systems (CHI '20)*. Association for Computing Machinery, New York, NY, USA, 1–12. https://doi.org/10.1145/3313831.3376847

[40] Pornthep Preechayasomboon and Eric Rombokas. 2021. Haplets: Finger-worn wireless and low-encumbrance vibrotactile haptic feedback for virtual and augmented reality. *Frontiers in Virtual Reality* 2 (2021), 738613. https://doi.org/10.3389/frvir.2021.738613

[41] Valentin Romero, Johan Lahti, Adrián Castaño Zambudio, Jurdan Mendiguchia, Pedro Jiménez Reyes, and Jean-Benoît Morin. 2022. Effects of Fatigue Induced by Repeated Sprints on Sprint Biomechanics in Football Players: Should We Look at the Group or the Individual? *International Journal of Environmental Research and Public Health* 19, 22 (Nov. 2022), 14643. https://doi.org/10.3390/ijerph192214643

[42] Jongman Seo and Seungmoon Choi. 2013. Perceptual analysis of vibrotactile flows on a mobile device. *IEEE transactions on haptics* 6, 4 (2013), 522–527. https://doi.org/10.1109/TOH.2013.24

[43] R Sharma. 2019. Effect of obliquity of incident light on the performance of silicon solar cells. *Heliyon* 5, 7 (2019), e01965. https://doi.org/10.1016/j.heliyon.2019.e01965

[44] Yuxiang Shi, Fan Wang, Jingwen Tian, Shuyao Li, Engang Fu, Jinhui Nie, Rui Lei, Yafei Ding, Xiangyu Chen, and Zhong Lin Wang. 2021. Self-powered electro-tactile system for virtual tactile experiences. *Science Advances* 7, 6 (Feb. 2021), eabe2943. https://doi.org/10.1126/sciadv.abe2943

[45] Bernd Strassner and Kai Chang. 2013. Microwave Power Transmission: Historical Milestones and System Components. *Proc. IEEE* 101, 6 (June 2013), 1379–1396. https://doi.org/10.1109/JPROC.2013.2246132

[46] Shan-Yuan Teng, K. D. Wu, Jacqueline Chen, and Pedro Lopes. 2022. Prolonging VR Haptic Experiences by Harvesting Kinetic Energy from the User. In *Proceedings of the 35th Annual ACM Symposium on User Interface Software and Technology (UIST '22)*. Association for Computing Machinery, New York, NY, USA, 1–18. https://doi.org/10.1145/3526113.3545635

[47] Shan-Yuan Teng, K. D. Wu, Jacqueline Chen, and Pedro Lopes. 2022. Prolonging VR Haptic Experiences by Harvesting Kinetic Energy from the User. In *Proceedings of the 35th Annual ACM Symposium on User Interface Software and Technology (UIST '22)*. Association for Computing Machinery, New York, NY, USA, 1–18. https://doi.org/10.1145/3526113.3545635

[48] Teslasuit. 2023. Full body haptic VR suit for motion capture and training. Retrieved May 15, 2023 from https://teslasuit.io/

[49] Ambuj Varshney, Andreas Soleiman, Luca Mottola, and Thiemo Voigt. 2017. Battery-free Visible Light Sensing. In *Proceedings of the 4th ACM Workshop on Visible Light Communication Systems (VLCS '17)*. Association for Computing Machinery, New York, NY, USA, 3–8. https://doi.org/10.1145/3129881.3129890

[50] Changsheng Wu, Aurelia C. Wang, Wenbo Ding, Hengyu Guo, and Zhong Lin Wang. 2019. Triboelectric Nanogenerator: A Foundation of the Energy for the New Era. *Advanced Energy Materials* 9, 1 (2019), 1802906. https://doi.org/10.1002/aenm.201802906

[51] Huiling Yu and Ke jin. 2021. Multi-target charging strategy for smartphones based on laser wireless power transmission and machine vision technology. *Journal of Physics: Conference Series* 1754, 1 (Feb. 2021), 012158. https://doi.org/10.1088/1742-6596/1754/1/012158

[52] Qingqing Zhang, Wen Fang, Qingwen Liu, Jun Wu, Pengfei Xia, and Liuqing Yang. 2018. Distributed Laser Charging: A Wireless Power Transfer Approach. *IEEE Internet of Things Journal* 5, 5 (Oct. 2018), 3853–3864. https://doi.org/10.1109/JIOT.2018.2851070

[53] Yang Zhang, Gierad Laput, and Chris Harrison. 2018. Vibrosight: Long-range vibrometry for smart environment sensing. In *Proceedings of the 31st Annual ACM Symposium on User Interface Software and Technology*. 225–236.

[54] Siyan Zhao, Ali Israr, Micah Fenner, and Roberta L Klatzky. 2017. Intermanual apparent tactile motion and its extension to 3D interactions. *IEEE transactions on haptics* 10, 4 (2017), 555–566.

[55] Xirui Zhu, Ke Jin, Qi Hui, Wenxiang Gong, and Dongqin Mao. 2021. Long-Range Wireless Microwave Power Transmission: A Review of Recent Progress. *IEEE Journal of Emerging and Selected Topics in Power Electronics* 9, 4 (Aug. 2021), 4932–4946. https://doi.org/10.1109/JESTPE.2020.3038166